

- those of the analogous A<sub>2</sub>/G reaction, as expected for the higher driving force reaction.
34. J. W. Evenson and M. Karplus, *Science* **262**, 1247 (1993); S. Priyadarshy, S. M. Risser, D. N. Beratan, *J. Bioinorg. Chem.* **3**, 196 (1998); J. J. Regan et al., *Chem. Biol.* **2**, 489 (1995).
35. W. B. Davis, W. A. Svec, M. A. Ratner, M. R. Wasielewski, *Nature* **396**, 60 (1998).
36. Alternatively, the nitrogen-to-carbon substitution in Z compared with the natural base may decrease the strength of stacking interactions for this modified base. However, the use of deazaadenine (which has an oxidation potential quite similar to that of G) as an electron donor in analogous experiments produced an interstrand distance dependence almost identical to that observed with G (S. O. Kelly and J. K. Barton, data not shown). Therefore, it appears that the increased distance dependence for the A<sub>2</sub>-Z reaction results from energetic effects.
37. S. Georgiou, T. D. Bradrick, A. Philippidis, J. M. Beechem, *Biophys. J.* **70**, 1909 (1996).
38. J. Jortner, M. Bixon, T. Langenbacher, M. E. Michel-Beyerle, *Proc. Natl. Acad. Sci. U.S.A.* **95**, 12759 (1998); A. K. Felts, W. T. Pollard, R. A. Freisner, *J. Phys. Chem.* **99**, 2929 (1995); A. Okada, V. Chernyak, S. Mukamel, *ibid.* **102**, 1241 (1998).
39. A<sub>e</sub>, A<sub>2</sub>, I, and Z phosphoramidites were all obtained from Glen Research. Oligonucleotides were prepared by standard automated techniques (with the exceptions described below) on a 394 ABI synthesizer and purified by reverse phase high-performance liquid chromatography. For Z, the oxidation step was carried out with 10-camphorsulfonyl oxaziridine as previously described (5). Base deprotection of etheno-adenine-containing oligonucleotides was carried out for 24 hours at room temperature. Oligonucleotides containing modified bases were characterized by electrospray mass spectroscopy. Samples were prepared as follows: on the basis of the calculated extinction coefficients for DNA sequences [ $\epsilon_{260}$  ( $M^{-1} \text{cm}^{-1}$ )]: dC =  $7.4 \times 10^3$ ; dG =  $12.3 \times 10^3$ ; dT =  $6.7 \times 10^3$ ; dA =  $15.0 \times 10^3$ ; dZ-G =  $10.5 \times 10^3$ ; dI =  $11.0 \times 10^3$ ; d(A<sub>e</sub>) =  $4.5 \times 10^3$ ; d(A<sub>2</sub>) =  $2.5 \times 10^3$ , appropriate amounts of complementary materials were combined at 1:1 stoichiometry and dissolved in 100 mM sodium phosphate (pH 7) to give a final duplex concentration of 100  $\mu\text{M}$ . The resulting solutions were heated to 90°C and slowly cooled to ambient temperature over 2 to 3 hours to anneal the duplex. The ultraviolet-visible spectra of the duplex samples were carefully measured to ensure that the absorbance at the excitation wavelength was identical for every sample. Thermal denaturation experiments were performed on a HP8452A diode array spectrophotometer with samples at a duplex concentration of 25  $\mu\text{M}$  in 100 mM phosphate (pH 7).
- Absorbance was monitored every 2°C with 3-min equilibration times. All duplexes used in these experiments exhibited cooperative thermal denaturation profiles with melting temperatures >25°C with 25  $\mu\text{M}$  duplex and therefore were fully hybridized under the conditions of all fluorescence experiments (100  $\mu\text{M}$ , 20°C).
40. Measurements were performed on a TCSPC apparatus previously described (4). Excitation was performed at 325 nm, and emission was monitored at 350 nm for A<sub>2</sub> and 400 nm for A<sub>e</sub>. Two data sets were obtained for each sample, one containing >10,000 counts for the determination of decay lifetimes, and another taken over a 120-s time interval to quantitate static quenching. Experiments were otherwise performed under the same conditions as steady-state experiments (100  $\mu\text{M}$  duplex, 100 mM sodium phosphate, pH 7).
41. C. Santhosh and P. C. Mishra, *Spectrochim. Acta* **47A**, 1685 (1991).
42. We thank E. Stemp for assistance with transient absorption experiments, R. Villahermosa for assistance with single-photon counting measurements, and T. Fiebig for discussions and assistance with molecular modeling. In addition, we acknowledge the NIH (grant GM49216 to J.K.B., predoctoral traineeship to S.O.K.) for financial support.

27 August 1998; accepted 7 December 1998

## Emergent Properties of Networks of Biological Signaling Pathways

Upinder S. Bhalla and Ravi Iyengar\*

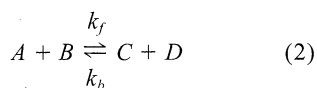
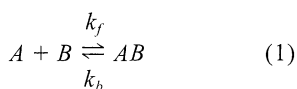
Many distinct signaling pathways allow the cell to receive, process, and respond to information. Often, components of different pathways interact, resulting in signaling networks. Biochemical signaling networks were constructed with experimentally obtained constants and analyzed by computational methods to understand their role in complex biological processes. These networks exhibit emergent properties such as integration of signals across multiple time scales, generation of distinct outputs depending on input strength and duration, and self-sustaining feedback loops. Feedback can result in bistable behavior with discrete steady-state activities, well-defined input thresholds for transition between states and prolonged signal output, and signal modulation in response to transient stimuli. These properties of signaling networks raise the possibility that information for "learned behavior" of biological systems may be stored within intracellular biochemical reactions that comprise signaling pathways.

Studies on the cyclic adenosine monophosphate (cAMP) signaling pathway led to the identification of several general mechanisms of signal transfer, such as regulation by protein-protein interactions, protein phosphorylation, regulation of enzymatic activity, production of second messengers, and cell surface signal transduction systems (1). These mechanisms of signal transfer have subsequently been shown to occur in many path-

ways, including Ca<sup>2+</sup> signaling pathways (2), tyrosine kinase pathways (3), and other protein kinase cascades, and recently in the intracellular protease cascades in apoptosis (4). Initially, signaling pathways were studied in a linear fashion, and it was shown that many important biological effects are obtained through linear information transfer. However, it has become increasingly clear that signaling pathways interact with one another and the final biological response is shaped by interaction between pathways. These interactions result in networks that are quite complex and may have properties that are nonintuitive. A systematic analysis of interactions between signaling pathways could be useful in understanding the properties of these networks. We developed models for simple net-

works consisting of up to four signaling pathways to determine if the network has properties that the individual pathways do not and if networking results in persistent activation of protein kinases after transient stimulus. Persistent activation of protein kinases is a general mechanism for eliciting biological effects. Cholera toxin continuously elevates cAMP, resulting in persistent activation of protein kinase A (PKA), inhibition of intestinal water reabsorption, and diarrhea, key pathological manifestations of cholera (5). Since this original demonstration, persistent activation of protein kinases has been implicated in diverse processes such as neoplastic transformation (6) and learning and memory (7). Although mutations or altered gene expression can result in persistent activation of protein kinases, we wished to ask the following question: Do connections between preexisting signaling pathways result in persistently activated protein kinases capable of eliciting end-point biological effects?

To develop models of signaling pathways, it is necessary to consider the mechanisms by which signal transfer occurs. In biological systems, signal transmission occurs mostly through two mechanisms: (i) protein-protein interactions and enzymatic reactions such as protein phosphorylation and dephosphorylation (ii) or protein degradation or production of intracellular messengers. In an approach that would include all of these reactions, we used the basic chemical reaction schemes of



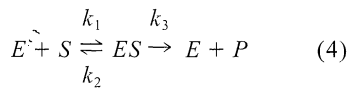
U. S. Bhalla, Department of Pharmacology, Mount Sinai School of Medicine, New York, NY 10029, USA, and National Centre for Biological Sciences, Post Office Box 1234, Bangalore 560012, India. R. Iyengar, Department of Pharmacology, Mount Sinai School of Medicine, New York, NY 10029, USA.

\*To whom correspondence should be addressed.

to represent all reactions. In this formulation, the interactions are completely specified by the rate constants ( $k_b$  and  $k_f$ ) and by the initial concentration of each reactant ( $A$ ,  $B$ ,  $C$ , and  $D$ ). All these equations are analytically equivalent and can be represented by differential equations of the form

$$d[A]/dt = k_b[C][D] - k_f[A][B] \quad (3)$$

The standard Michaelis-Menten formulation for enzymes is a special case of the two reactions in sequence, with the assumption that the final step is irreversible:



This is specified by three rate constants,  $k_1$ ,  $k_2$ , and  $k_3$ , and the initial concentrations of enzyme  $E$ , substrate  $S$ , and product  $P$ . Addition of further reactants or alterations of kinetic parameters (or both) during time course analysis can be accommodated within this framework. All parameters used in these models were derived from published experimental studies. In most cases, measurements in the literature allowed us to cross check the values of the constants we used. The constants used in the various pathways models and the details of their derivation are de-

scribed in the supplementary material on the *Science* Web site ([www.sciencemag.org/feature/data/982608.shl](http://www.sciencemag.org/feature/data/982608.shl)) and the Iyengar laboratory Web site (8). All numerical computations were performed as described (9).

Initially, model activation of single components was set up. The objective in generating the model for an individual signaling pathway was to obtain a good empirical model that accurately fit the available experimental data. Many signaling pathways are influenced by multiple stimuli often acting synergistically. In such cases, an iterative procedure was followed to ensure that the model replicated experimental results. For example, the details of synergistic activation of protein kinase C (PKC) by multiple ligands are shown at our Web site (8). We developed a library of models for different signaling pathways. In all cases, the invariant criterion was that the model for the individual pathway yield responses very similar to the experimentally obtained data. The reactions for the individual models are given in Fig. 1. The rate constants and papers from which they are derived are available on our Web site (8). A compartmental model of a hippocampal CA1 neuron was implemented in GENESIS, and calcium influx through *N*-methyl-D-aspartate (NMDA) channels on a dendritic spine on the model was computed with previously published

parameters (10). Synaptic input was delivered to this model to match a protocol commonly used to elicit long-term potentiation (LTP): three tetanic bursts at 100 Hz, for 1 s each, separated by 600 s. The  $\text{Ca}^{2+}$  waveform generated by this simulation was fed into the kinetic model. The kinetic model was insensitive to the value of  $\text{Ca}^{2+}$  amplitude within a factor of two.

We developed the network model in stages. We modeled individual pathways first, and then we examined experimentally defined combinations of two or three such individual pathways and tested these combined models against published data. We repeated this process using larger assemblies of pathways until the entire network model of interacting pathways was formed. Pathways were linked by two kinds of interactions: (i) Second messengers such as arachidonic acid (AA) and diacylglycerol (DAG) produced by one pathway were used as inputs to other pathways. (ii) Enzymes whose activation was regulated by one pathway were coupled to substrates belonging to other pathways. In establishing connections between pathways, we only used mechanisms that had been described experimentally.

As an example of one signaling pathway, we modeled epidermal growth factor (EGF) stimulation of mitogen-associated protein ki-

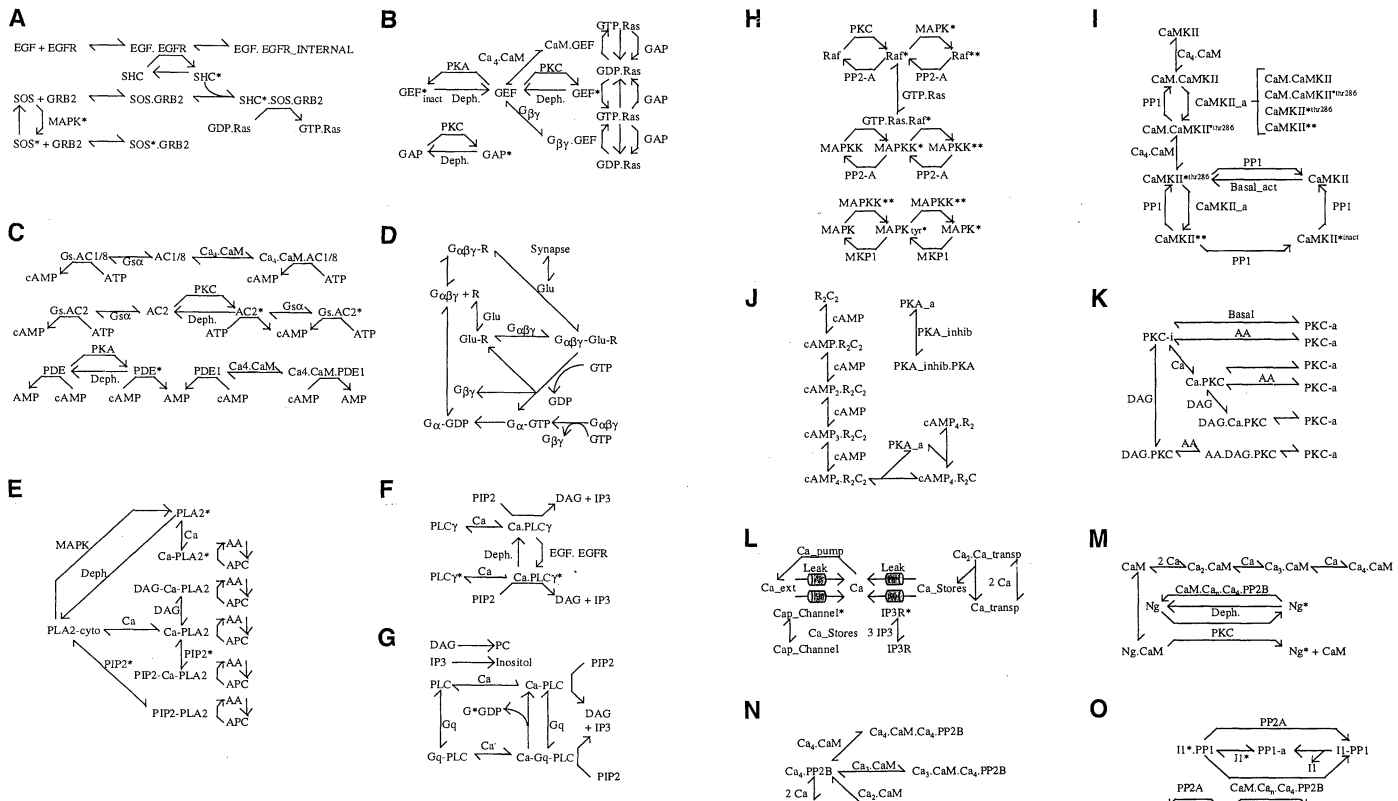


**Fig. 1.** Reaction schemes and parameters for library of pathways in simulations. Reversible reactions are represented as bidirectional arrows and irreversible reactions as unidirectional arrows. Enzyme reactions are drawn as an arrow with two bends, where the enzyme is located on the middle segment. For clarity, the same reactant may be represented multiple times in a given reaction scheme, but it is modeled only as a

single reactant. Details of parameters for the reactions and references are available at our Web site (8).

nases (MAPK) 1 and 2 and EGF activation of phospholipase C- $\gamma$  (PLC $\gamma$ ) (Fig. 2A) using reaction schemes in Fig. 1, A, B, H, and F. In Fig. 2B, the time course of activation of MAPK by EGF is shown. Here, we compared the experimental data (solid triangles) from experiments by Teng *et al.* (11) with the values obtained from the model (open triangles). It can be readily seen that the model accurately reproduces the experimentally observed data. A second example is shown in Fig. 2C. Here, EGF stimulation of PLC $\gamma$  is measured at various  $\text{Ca}^{2+}$  concentrations and compared against experimental data obtained by Wahl *et al.* (12). Again, the model provides a good fit to the experimentally observed activation.

The next stage of analysis used two interconnected pathways. Here, two types of connections were studied. The first type involves a feedback loop. Persistently activated MAPK can trigger proliferation and in some

cell types is sufficient to induce transformation (13). We determined if sustained MAPK activation could occur after an extracellular signal is withdrawn. For this signal, flow from EGF receptor through two interconnected pathways, the PLC $\gamma$ -PKC pathway and Ras-Raf-MAPK pathways, was analyzed. The two pathways interact at two points. PKC activates Raf (14). MAPK can phosphorylate and activate cytosolic phospholipase A-2 (cPLA $_2$ ) (15), and the AA produced by cPLA $_2$  acts synergistically with DAG to activate PKC (16). These connections should result in a positive feedback loop.

In such a system, one can determine the amplitude and duration of the extracellular signal required to obtain sustained activation of the system. In this simulation, the system was exposed to 2 or 5 nM EGF for either 10 or 100 min. Only the 5 nM stimulation at 100

min results in active MAPK or PKC even after the signal was withdrawn. The other two conditions result in deactivation of the system soon after the external signal is withdrawn (Fig. 2D). The reason for this difference can be understood by analysis of a plot of active PKC versus MAPK, as shown in Fig. 2E. This plot is formed by the concentration-effect curves of MAPK activation of PKC (dashed line) and PKC activation of MAPK (solid line), plotted on the same axes. The curves for PKC versus MAPK and MAPK versus PKC intersect at three points, A, B, and T. Point A represents high activity for both PKC and MAPK, whereas point B represents low activity. Both of these points represent distinct steady-state levels. Such a system with two distinct steady states is a bistable system. The bifurcation point T is important because it defines threshold stimulation. As the concentration-effect curves are

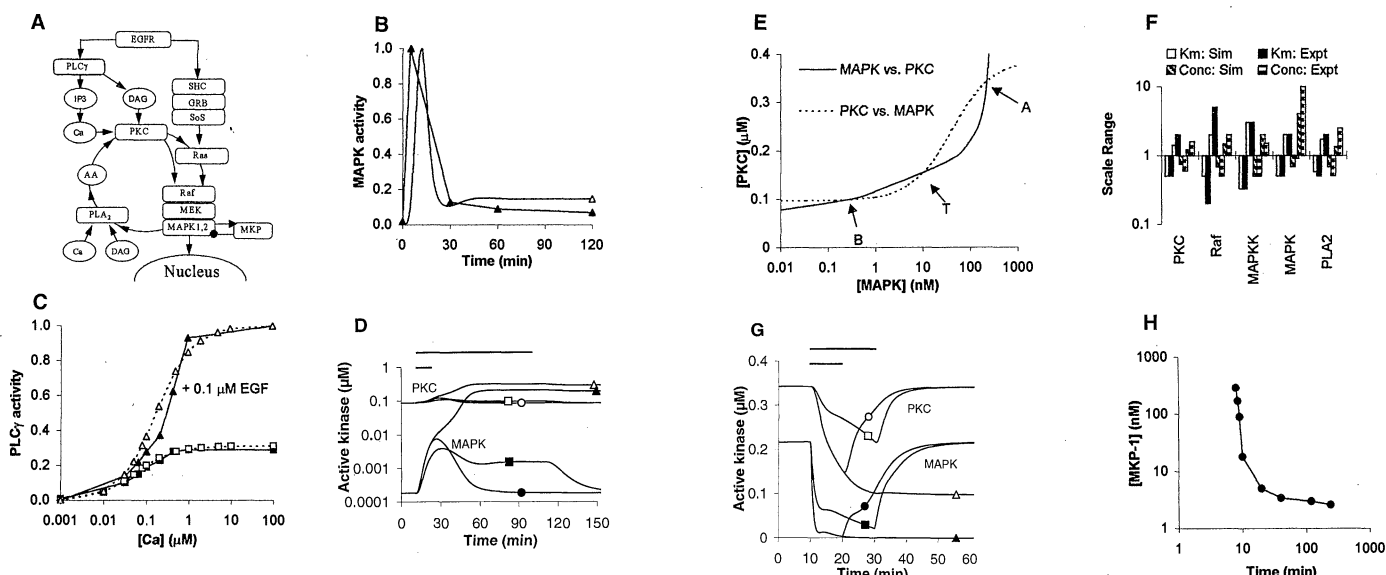


**Fig. 2.** EGF receptor signaling pathways. (A) Block diagram of signaling pathways. Rectangles represent enzymes, and circles represent messenger molecules. This model used modules shown in Fig. 1, A, E, B, F, H, K, and L from the library of models. (B and C) Matching models to experiments. (B) Predicted (open triangle) and experimental (filled triangles) time course of response of MAPK to a steady EGF stimulus of 100 nM. The fall in the MAPK activity after the initial stimulation is due to a combination of EGF receptor internalization and MAPK phosphorylation and inactivation of SoS. (C) Concentration-effect curves for activation of PLC $\gamma$  by  $\text{Ca}^{2+}$  in the presence (triangles) or absence (squares) of EGF. Dashed lines are model data, and solid lines are experimental data. In (B) and (C), the y axis represents fractional activation. (D to H) Activation of the feedback loop by EGF receptor. (D) Activation of feedback loop by EGF. PKC (open symbols) and MAPK (filled symbols) are monitored to show status of feedback. Three stimulus conditions are represented: 10 min at 5 nM EGF (short bar, circles), 100 min at 2 nM EGF (long bar, squares), and 100 min at 5 nM EGF (long bar, triangles). Only the third condition succeeds in causing activation of the feedback loop. (E) Bistability plot for feedback loop represented in (A). The PKC versus MAPK plot (dashed line) was constructed by holding the level of active MAPK fixed, running the simulation until steady state, and reading the value for active PKC. This was continued for a series of MAPK levels spanning the range of interest. The process is repeated for MAPK versus PKC (solid line) by holding active PKC at a fixed level and monitoring resultant MAPK levels. Both plots are drawn with PKC on the y axis and MAPK on the x

axis. The curves intersect at three points: B (basal), T (threshold), and A (active). A and B are stable points, and T is metastable. (F) Estimated experimental uncertainty in enzyme parameters, compared with simulated range over which bistability is observed. Bistability is present over a range comparable to the experimental uncertainty, indicating that the phenomenon is robust. Black bars, experimental uncertainty in the Michaelis constant ( $K_m$ ); white bars, simulated bistability range for  $K_m$ ; horizontal stripes, experimental uncertainty in concentration; diagonal stripes, simulated bistability range for concentrations. MAPK has a particularly large uncertainty in concentration range because of large differences in tissue distributions. (G) Inactivation of feedback loop by MKP-1. PKC (open symbols) and MAPK (filled symbols) are monitored to show status of feedback. The feedback loop was initially activated by a suprathreshold stimulus shown at our Web site (8), and then one of three inhibitory inputs was applied: 10 min at 8 nM (short bar, circles), 20 min at 4 nM (long bar, squares), and 20 min at 8 nM (long bar, triangles). Only the third condition is able to inactivate the feedback loop. The rebound in the first two cases is due to two factors: the persistence of AA due to a relatively slow time course of removal and the time course of dephosphorylation of activated kinases in the MAPK cascade. (H) Thresholds for inactivation of feedback loop. MKP was applied for varying times and amounts. At high MKP levels, inactivation occurs more quickly, but there is a minimum threshold of nearly 10 min. Conversely, when MKP is applied for very long times, at least 2 nM MKP is required to inactivate the feedback loop.

steady-state relations, the threshold T is rigorously defined only for steady-state situations. However, as an approximation, if the initial stimulation (amplitude and duration) is such that either PKC or MAPK is activated above the level T, then the system will reach steady state at point A. In contrast, if the initial stimulation is below T, then the system upon removal of stimulus will relax to the level B, which would be the basal amount of activity.

Such a bistable system has the potential to store information, and in fact an important class of computer memory (static RAM) is based on bistable devices. Signaling events that push the levels of either activated PKC or activated MAPK past the intersection point T will cause the system to flip from one state to another. This analysis can be generalized to any combination of pathways in a feedback loop. Not all feedback systems will exhibit concentration-effect curves that intersect at three points to produce bistability. Single intersection points will produce a system with only one stable state. Even numbers are biochemically implausible, and higher numbers (5, 7, and so forth) of intersections are unlikely to occur because of the shape of most concentration-effect curves. It is noteworthy that many biochemical dose-response curves take the shape most likely to produce a bistable system: a sigmoid. To determine the robustness of the model, we varied the constants for the various key enzymes in both directions. The bistable behavior was robust over a range of kinetic parameters (Fig. 2F). For several components, the bistable behavior was robust over a 100% range in either direction, but for PKC concentration the range was  $\pm 30\%$ . This may be due to the limited number of PKC isoforms used in our model.

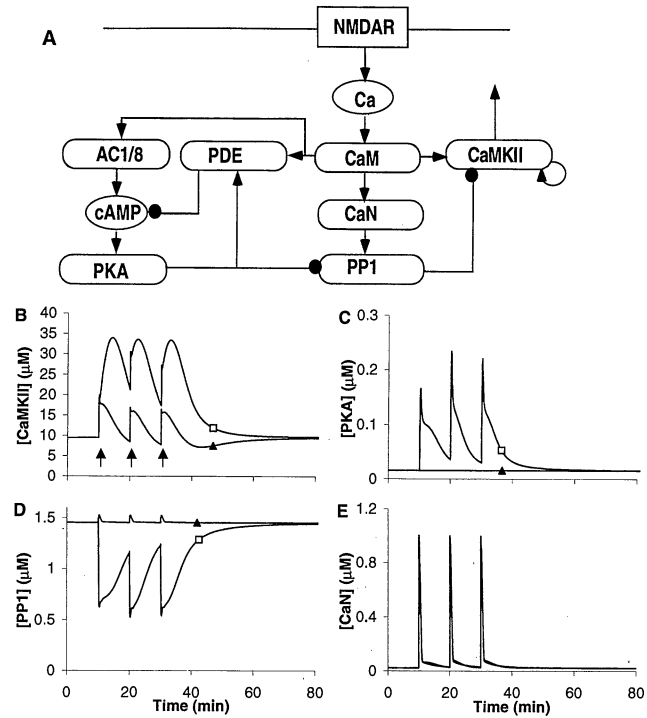
We also explored deactivation of this bistable system. MAPK is dephosphorylated by a very specific phosphatase, MAPK phosphatase 1 (MKP) (17). In the simulation in Fig. 2G, we examined the consequences of 8 nM MKP active for 10 or 20 min and 4 nM MKP active for 20 min. The active system fully relaxes only when 8 nM MKP is active for 20 min. Lower concentrations of MKP or shorter duration of application result in the system returning to steady-state activity at the higher level. The relation between the concentration of MKP and the duration of its action required to deactivate the system is shown in Fig. 2H. Thus, the emergent properties of this feedback system define not only the amplitude and duration of the extracellular signal required to activate the system but also the magnitude and duration of processes such as phosphatase action required to deactivate the system. These properties make a feedback system such as this one, once activated, capable of delivering a constant

output in a manner unaffected by small fluctuations caused by activating or deactivating events. This capability to deliver a stimulus-triggered constant output signal even after the stimulus is withdrawn may have numerous biological consequences.

The second mode of interaction between the two pathways we analyzed was the gate (18).  $\text{Ca}^{2+}$ /calmodulin-dependent protein kinase II (CaMKII) functions in LTP of synaptic responses in the hippocampus. Persistent activation of CaMKII in the postsynaptic CA1 neuron increases synaptic responses (19). CaMKII can be activated in a persistent manner by autophosphorylation at Thr<sup>286</sup> even after the ambient  $\text{Ca}^{2+}$  concentration drops (20), and transgenic mice expressing CaMKII in which Thr<sup>286</sup> is converted to Ala have impaired hippocampal LTP (21). Certain forms of LTP also require the cAMP pathway (22). Although postsynaptic cAMP is required, by itself it does not alter postsynaptic responses. On the basis of these observations, we had proposed that the cAMP pathway gates CaMKII signaling through the regulation of protein phosphatases (18). With the inflow of  $\text{Ca}^{2+}$ ,  $\text{Ca}^{2+}$ /calmodulin (CaM) not only activates CaMKII and calcineurin (CaN, also known as PP2B) but also elevates intracellular cAMP through CaM-dependent activation of adenylyl cyclases 1 and 8 (AC1-AC8) (23). We tested whether interactions between CaMKII, the cAMP pathway, and CaN are sufficient to produce prolonged acti-

vation of CaMKII even after the  $\text{Ca}^{2+}$  signal is terminated (Fig. 3A). An initial stimulus similar to one that produces cAMP-dependent LTP was applied, and the activities of four key enzymes [CaMKII, PKA, protein phosphatase 1 (PP1), and CaN] were calculated. The concentrations of the active enzymes are shown in Fig. 3, B to E. The initial increase in intracellular  $\text{Ca}^{2+}$  caused an activation of CaMKII, AC1, and CaN through CaM binding and of PKA through increase in cAMP produced through activation of AC1-AC8. The simulations predict that activation of AC1-AC8 overcomes competing degradation of cAMP because of activation of CaM-dependent and PKA-activated PDEs. PKA activation leads to phosphorylation of the Inhibitor-1 protein and hence to the inhibition of PP1 (24). When intracellular concentration returns to normal, both PKA and CaN are rapidly deactivated. The balance of basal activity of PKA and CaN ensures that PP1 is restored to full activity within 20 min of the stimulus. As PP1 becomes active, it is able to dephosphorylate CaMKII at Thr<sup>286</sup>. This deactivates CaMKII (25). Thus, the system returns to basal state within 20 min of the final  $\text{Ca}^{2+}$  influx. The presence of a cAMP-operated gate leads to a large increase in the amplitude of the CaMKII response and prolongation of its activity, as is shown in Fig. 3B. Nevertheless, it does not lead to a persistent activation of CaMKII. The balance of CaMKII autophosphorylation, dephosphorylation, and relative activities of PP1 and CaN do, however, lead to a prolonga-

**Fig. 3.** CaMKII regulation. (A) Block diagram of modeled pathways. NMDAR and Ca influx are modeled in a compartmental model of a CA1 neuron with a series of three tetanic stimuli at 100 Hz, lasting 1 s each, separated by 10 min. This model used modules shown in Fig. 1, C, I, J, M, N, and O, from the library. (B to E) Activation of enzymes coupled to CaMKII. Open squares, full model; filled triangles, cAMP is held fixed at resting concentrations, thereby preventing rise in PKA activity. (B) Activation of CaMKII. The arrows represent tetanic stimuli at 10, 20, and 30 min. CaMKII levels as well as time course are decreased when cAMP is held fixed. (C) Activation of PKA. PKA activity rises sharply because of AC1-AC8 binding to Ca/CaM and producing cAMP. (D) Activity of PP1. PKA activation causes PP1 activity to fall to less than half its resting level. The small transients when cAMP is fixed are because of CaN activation of PP1 due to Ca/CaM elevation. (E) CaN (PP2B) activation by Ca/CaM elevation. The full model-cAMP fixed curves overlap almost perfectly.



tion of CaMKII activity for 20 min after the stimulus was withdrawn, which may in some situations be sufficient to trigger a physiological response.

We next developed a model for interaction between four signaling pathways. The response to the neurotransmitter glutamate at input synapses of hippocampal CA1 neurons involves multiple signaling pathways. Glutamate in combination with postsynaptic depolarization triggers the inflow of  $\text{Ca}^{2+}$  through the NMDA receptor (26). The postsynaptic protein kinases known to be activated through  $\text{Ca}^{2+}$  influx through the NMDA receptor include CaMKII, PKC, PKA, and MAPK. The PKC and MAPK pathways are linked as are the CaMKII and cAMP pathways. The PKC pathway is also connected to the cAMP pathway in the hippocampus through AC2, which can be phosphorylated and activated by PKC (27). These connections suggest that the four protein kinase pathways can form a network (Fig. 4A).

The behavior of this network was analyzed to determine if it was possible to sustain CaMKII activity after the initial glutamate-induced  $\text{Ca}^{2+}$  inflow was terminated. The concentrations of key enzymes in the system were plotted as a function of time (Fig. 4, B to G). In all cases, the profile of the active state was analyzed in the presence and absence of the feedback loop, created by the connection between the PKC and MAPK pathways mediated by cPLA<sub>2</sub>. The profiles in Fig. 4, B and C, represent time courses of activation of PKC and

MAPK, respectively. Initially, there are spikes of PKC activation due to the inflow of  $\text{Ca}^{2+}$  and activation of phospholipase C- $\beta$  (PLC $\beta$ ) to produce DAG. Activation of PKC resulted in activation of MAPK through Ras and Raf. If cPLA<sub>2</sub> was held at basal activity, the feedback loop was not established, and both PKC and MAPK activities returned to baseline after the stimulus was withdrawn. However, when the feedback loop was active, after the initial spike, there was a second rise in PKC activity that resulted from stimulation by DAG and AA (Fig. 4B). This resulted in a steady rise in MAPK activity that was persistent (Fig. 4C). PKA also showed initial spikes of activity caused by the stimulation of AC1 and AC8 by  $\text{Ca}^{2+}$  inflow. When the feedback loop was active, there is then a second smaller increase due to activation of AC2 by PKC (27). Because PKC activation is sustained, this stimulation of AC2 by PKC results in sustained PKA activation as well, albeit at a lower activity than that produced by Ca-stimulated transients (Fig. 4D). These connections suggest that the four protein kinase pathways can form a network (Fig. 4A).

PKA modulates the autophosphorylation state of CaMKII through regulation of PP1 (18). Inflow of  $\text{Ca}^{2+}$  led to initial bursts of CaMKII activity. If the feedback loop was not present, this activity slowly returned to basal levels. However, when the feedback loop was present, then the CaMKII activity reached steady state with a nearly twofold increase in the amount of active enzyme (Fig. 4E). The cause of the sustained increase in CaMKII activity within this network becomes obvious when the activity profiles of the two relevant

protein phosphatases are analyzed. PP1, which dephosphorylates CaMKII at the Thr<sup>286</sup> position, is initially inhibited through the spikes in PKA activity. The decrease in PP1 activation contributes to a net rise in CaMKII activity as basal activation (Fig. 1I) remains unchanged. PKA activity then falls considerably but settles at a higher steady-state level than the basal state as described above. PP1 activity therefore reaches a steady state at a lower level because of the sustained PKA activity (Fig. 4F).

In contrast, PP2B reaches a peak activity with the inflow of  $\text{Ca}^{2+}$ , but because it is not affected by other components of this network it returns to its inactive state upon removal of the  $\text{Ca}^{2+}$  signal (Fig. 4G). Its effect on PP1 activity is thus limited to the duration of the initial signal. Thus, a network can produce sustained protein kinase activity after an initial stimulus. Such sustained activities do not require any change in protein expression. They occur solely through the biochemical properties of the system under conditions at which the total concentrations of the reactants are fixed. This may correspond to the situation in the early phase of LTP (28). Because MKP induction can trigger turnoff of the feedback loop, MKP may act as a timer for feedback activity in a synapse, to mark the end of early LTP. Other transcriptional events could be initiated in parallel with MKP induction, and these gene products would be expected to reach the active synapse along with MKP. We suggest that the active feedback loop may gate incorporation of these products into the cytoskeleton. This may provide a mecha-

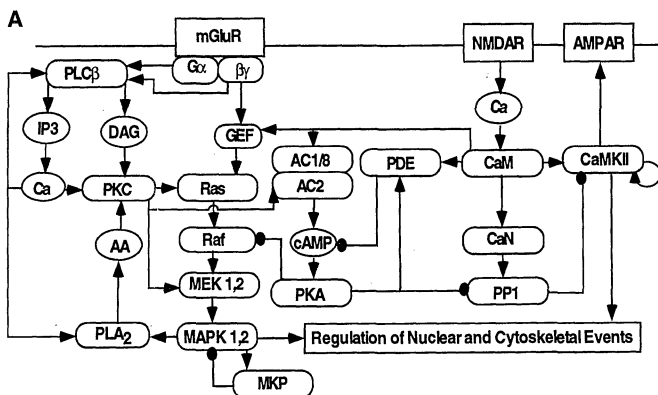
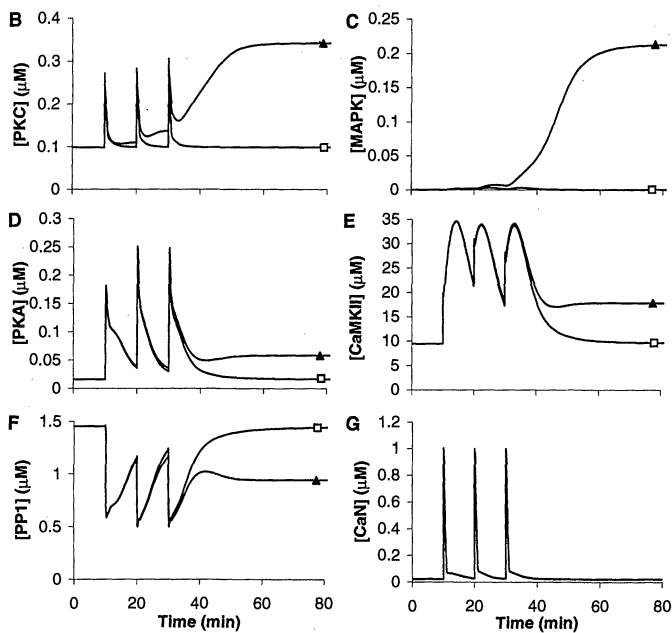


**Fig. 4.** Combined model with feedback loop, synaptic input, and CaMKII activity and regulation. (A) Block diagram of model. Two possible end points of the model are represented as  $\alpha$ -amino-3-hydroxy-5-methyl-4-isoxazolepropionate receptor-channel regulation and regulation of nuclear and cytoskeletal events. This model used all of the modules in the library except the module in Fig. 1A. (B to G) Activity profile of major enzymes in pathway with full model (filled triangles) and with feedback blocked by holding AA fixed at resting concentrations (open squares). (B) Activity profile of PKC. When feedback is present, successive spikes become larger. However, in the absence of feedback, PKC has a time course that returns to baseline in the interval between stimuli. (C) Activity profile of MAPK. Activity accumulates only in the presence of feedback to lead to turn on. (D) Activity profile of PKA. The Ca-stimulated waveforms are almost identical, but the baseline rises when feedback is on, because of PKC stimulation of AC2 and production of additional cAMP. (E) Activity profile of CaMKII. Again, the Ca-stimulated



waveforms are almost identical, but when feedback is present the baseline rises almost twofold. (F) Activity profile of PP1. The Ca stimulated waveforms overlap, but sustained PKA activity in the presence of feedback causes the baseline activity of PP1 to fall. This in turn leads to the rise in CaMKII activity in (E). (G) Activity profile of CaN (PP2B). This is unaffected by the presence or absence of feedback.

nism for selectively targeting gene products only to synapses receiving LTP-inducing stimuli (29). In this manner, the feedback loop might act as a bridge between extremely short stimuli and longer term synaptic change and also between local synaptic events and cell-wide production of synaptic proteins.

Networking results in several emergent properties that the individual pathways do not have. These properties include the following: (i) Extended signal duration. The coupling of fast responses to the slow responses confers on the system the ability to regulate output for considerable periods after withdrawal of the initial signal. (ii) Activation of feedback loops. Feedback interactions occur commonly in biochemical processes. Many metabolic pathways are regulated by end-point feedback inhibition. Here, a positive feedback system involving PKC and MAPK was analyzed. This feedback loop has some noteworthy features. Sustained PKC activity results from initial activation of PKC by  $\text{Ca}^{2+}$  and DAG and later activation due to synergy between AA and basal concentrations of DAG. AA concentrations are raised by the activation of cPLA2 by MAPK, which is stimulated indirectly by PKC. Thus, multiple modes ( $\text{Ca}^{2+}$  and DAG and DAG and AA) of stimulating PKC are essential for the feedback loop. The magnitude and duration of the feedback loop are limited by the concentrations of the components of the system and other reactions that impinge on components of the feedback loop. The sequential phosphorylation reactions in the MAPK cascade are targets for regulation by protein phosphatases. MAPK is known to induce MKP, which is relatively specific for MAPK. In our model, MKP is effective in turning off the fully activated feedback loop under appropriate conditions. Additionally, down-regulation of PKC could also turn off the loop. Thus, both MKP and PKC levels could be determinants of CaMKII activity, connections not intuitively obvious in the absence of the network. (iii) Definition of threshold stimulation for biological effects. Signals of defined amplitude and duration are required to evoke a physiological response. Some of the parameters that define threshold stimulation can be ascertained from this analysis of signaling networks. From Fig. 2, D and E, it can be readily seen that signals of sufficient amplitude and duration are required such that the initial PKC activity rises above the second intersection point T so that the feedback loop becomes operational and sustained PKC and MAPK activity is obtained. Corresponding thresholds are seen in the inactivation process (Fig. 2, G and H). Thus, the system (that is, the network) defines what the threshold stimulation will be and which external stimuli would be capable of evoking a biological response. (iv) Multiple signal outputs. Multiple signal outputs from a network may provide a safety mechanism to ensure that only appropriate signals are trans-

lated into alterations in biological behavior. Such a safety mechanism could use hierarchical phosphorylations as a requirement for evoking a response. The multiple protein kinases required for hierarchical phosphorylation would ensure that the biological response is obtained only when the network is fully operational and all of the output protein kinases are functional.

The intricacy and variety of biological signaling networks often defy analyses based on intuition. System properties are often dependent on subtle timing relations and competition between negative and positive regulators. Given the wealth of biochemical data, a computational analysis is well suited to handling both the complexity of multiple signaling interactions and the fine quantitative details. Such a model facilitates "thought experiments" on involved signaling pathways to predict hierarchies, which can then be experimentally tested. For instance, in LTP, the interrelations between several protein kinases are ill defined. Our model suggests that PKA is downstream of both PKC and MAPK and upstream with respect to CaMKII regulation (Fig. 4A). The model also provides a framework for understanding biological consequences of multiple modes of stimulating a single component. This is exemplified by our analysis of PKC, which is activated synergistically by  $\text{Ca}^{2+}$ , DAG<sup>+</sup>, and AA. The capability to be activated by multiple signals enables both the initial triggering of the kinase and its subsequent involvement in a feedback loop with bistable properties. Similarly, such models provide insights into the possible roles of isoform diversity. In Fig. 4A, our model uses both the CaM-stimulated AC1 and the PKC-activated AC2. The first adenylyl cyclase isoform allows the system to achieve a rapid inhibition of PP1 after  $\text{Ca}^{2+}$  influx. The second adenylyl cyclase isoform then provides a sustained inhibition of PP1 leading to prolonged CaMKII activation. Without AC2, the feedback loop would not be connected to PP1 regulation, and it would not be possible to sustain CaMKII activation after the  $\text{Ca}^{2+}$  signal is terminated.

The modeling of biological networks has several limitations. Emerging data indicate that signaling systems are often anchored and clustered, and thus both location and accessibility need to be quantitatively accounted for. Currently, experimental data to deal with these issues do not exist. The biochemical parameters come from purified components, and there is no definitive proof that these constants are unaltered with the cell. Given these uncertainties, models such as these should not be considered as definitive descriptions of networks within the cell, but rather as one approach that allows us to understand the capabilities of complex systems and devise experiments to test these capabilities.

The networks we propose may play a role

in LTP, a neural paradigm for some types of learning, and in proliferative "memory." It is possible that similar approaches, using other signaling pathways, can be used to explain aspects of developmental and immunological memories. In conclusion, these studies indicate that simple biochemical reactions can, with appropriate coupling, be used to store information. Thus, reactions within signaling pathways may constitute one locus for the biochemical basis for learning and memory.

#### References and Notes

- E. W. Sutherland and W. D. Wosilait, *Nature* **175**, 169 (1955); E. G. Krebs and E. H. Fischer, *J. Biol. Chem.* **218**, 483 (1956); M. Rodbell *et al.*, *ibid.* **246**, 1877 (1971); T. Pueffer, *ibid.* **252**, 7244 (1977); E. M. Ross and A. G. Gilman, *ibid.*, p. 6966.
- M. J. Berridge, *Annu. Rev. Biochem.* **56**, 159 (1987); *Nature* **361**, 315 (1993); D. E. Clapham, *Cell* **80**, 259 (1995).
- J. Schlessinger and A. Ullrich, *Neuron* **9**, 383 (1992).
- A. Ashkenazi and V. M. Dixit, *Science* **281**, 1305 (1998).
- C.-Y. Lai, *Crit. Rev. Biochem.* **9**, 171 (1980).
- T. Hunter, *Cell* **64**, 249 (1991).
- T. V. P. Bliss and G. L. Collingridge, *Nature* **361**, 31 (1993).
- The Iyengar laboratory Web site can be found at [piris.pharm.mssm.edu/urilab/](http://piris.pharm.mssm.edu/urilab/)
- All numerical computations were performed with the kinetics library, which is an extension to GENESIS, the General Neural Simulation System (30). The exponential Euler formulation was used for integration. Computations were carried out with the "well-stirred" assumption, that is, that all molecules had equal access to all others. All computations were carried out with the actual number of available molecules, rather than their concentrations. This procedure allows for computations for membrane-bound proteins and molecules. The numerical accuracy of the computations was verified in three ways: (i) Simple kinetic schemes that could be calculated analytically were modeled, and simulated results were compared with the analytical results. (ii) The law of mass conservation and microscopic reversibility principles were used as tests of accuracy in complex reaction schemes. (iii) The same model was run at different time steps, and the resulting simulated values were compared. The calculations were shown to be stable and to provide convergent solutions for the range of time steps used in the study. Computations were carried out on Sun workstations and on PCs running Linux. A graphical user interface Kinetikit was built with the standard GENESIS graphical interface components. The interface does not affect the underlying calculations but was very useful in setting up reactions in an error-free manner and rapidly testing the behavior of different models. The interface was also crucial to the process of managing the enormous amounts of data involved. GENESIS, Kinetikit, and the library of models are available on the network (8).
- R. D. Traub *et al.*, *J. Neurophysiol.* **66**, 635 (1991); W. R. Holmes and W. B. Levy, *ibid.* **63**, 1148 (1990); E. De Schutter and J. M. Bower, *Neural Comput.* **51**, 681 (1993).
- K. K. Teng *et al.*, *J. Biol. Chem.* **270**, 20677 (1995).
- M. I. Wahl *et al.*, *ibid.* **267**, 10447 (1992); S. Nishizuka *et al.*, *Science* **250**, 1253 (1990).
- S. A. Aaronson, *Science* **254**, 1146 (1991); C. J. Marshall, *Cell* **80**, 179 (1995).
- W. Kolch *et al.*, *Nature* **364**, 249 (1993); M. P. Carroll, and W. S. May, *J. Biol. Chem.* **269**, 1249 (1994).
- L. L. Lin *et al.*, *Cell* **72**, 269 (1993); R. A. Nemenoff *et al.*, *J. Biol. Chem.* **268**, 1960 (1993).
- Y. Nishizuka, *Science* **258**, 607 (1992); T. Shinomura *et al.*, *Proc. Natl. Acad. Sci. U.S.A.* **88**, 5149 (1991).
- J.-M. Brondello *et al.*, *J. Biol. Chem.* **272**, 1368 (1997); C. H. Charles *et al.*, *Proc. Natl. Acad. Sci. U.S.A.* **90**, 5292 (1993).
- R. D. Blitzer *et al.*, *Neuron* **15**, 1403 (1995); R. Iyen-

- gar, *Science* **271**, 461 (1996); R. D. Blitzer *et al.*, *ibid.* **280**, 1940 (1998).
19. D. L. Pettit, S. Perlman, R. Malinow, *Science* **266**, 1881 (1994); J.-H. Wang and P. Kelly, *Neuron* **15**, 443 (1995); P.-M. Lledo *et al.*, *Proc. Natl. Acad. Sci. U.S.A.* **92**, 11175 (1995).
  20. S. G. Miller and M. B. Kennedy, *Cell* **44**, 861 (1986); C. M. Schworer *et al.*, *J. Biol. Chem.* **263**, 13486 (1988); P. I. Hanson and H. Schulman, *Annu. Rev. Biochem.* **61**, 559 (1992); T. Meyer *et al.*, *Science* **256**, 1199 (1992).
  21. K. P. Giese *et al.*, *Science* **279**, 870 (1998).
  22. U. Frey, Y.-Y. Huang, E. R. Kandel, *ibid.* **260**, 1661 (1993); P. V. Nguyen, T. Abel, E. R. Kandel, *ibid.* **265**, 1104 (1994).
  23. D. M. Chetkovich *et al.*, *Proc. Natl. Acad. Sci. U.S.A.* **88**, 6467 (1991); D. M. Chetkovich and J. D. Sweatt, *J. Neurochem.* **61**, 1933 (1993); R. Iyengar, *FASEB J.* **7**, 563 (1993); D. M. F. Cooper, N. Mons, J. W. Karpen, *Nature* **374**, 421 (1995).
  24. S. Shinolikar and A. C. Nairn, *Adv. Second Messenger Phosphoprotein Res.* **23**, 1 (1991).
  25. J. Lisman, *Trends Neurosci.* **17**, 406 (1994).
  26. S. Hestrin *et al.*, *J. Physiol.* **422**, 302 (1990).
  27. O. Jacobowitz *et al.*, *J. Biol. Chem.* **268**, 3829 (1993); K. D. Lustig *et al.*, *ibid.*, p. 13900; M. Yoshimura and D. M. F. Cooper, *ibid.*, p. 4604; O. Jacobowitz and R. Iyengar, *Proc. Natl. Acad. Sci. U.S.A.* **91**, 10630 (1994).
  28. U. Staubli and D. Chun, *J. Neurosci.* **16**, 853 (1996).
  29. U. Frey and R. G. M. Morris, *Nature* **385**, 533 (1997); E. Schuman, *Neuron* **18**, 339 (1997).
  30. U. S. Bhalla, in *The Book of GENESIS, Exploring Realistic Neural Models with General Neural Simulation System*, J. M. Bower and D. Beeman, Eds. (Springer-Verlag, Berlin, ed. 2, 1998), chap. 10.
  31. We thank L. Birnbaumer, A. Karlin, E. Marder, and M. Rodbell for reading earlier versions of this paper and J. Lisman for a critical review of our work. We are also very grateful to G. Weng and P. Ram and other members of the Iyengar laboratory for all help with this paper. U.S.B. was an Aaron Diamond Fellow, and this work was supported in part by a fellowship from the Aaron Diamond Foundation and NIH grant GM-54508. This paper is dedicated to the memory of Martin Rodbell.

18 May 1998; accepted 3 December 1998

## Role of DNA 5-Methylcytosine Transferase in Cell Transformation by *fos*

A. V. Bakin and T. Curran\*

The *Fos* and *Jun* oncogenes form dimeric complexes that stimulate transcription of genes containing activator protein-1 regulatory elements. We found, by representational difference analysis, that expression of DNA 5-methylcytosine transferase (*dnmt1*) in *fos*-transformed cells is three times the expression in normal fibroblasts and that *fos*-transformed cells contain about 20 percent more 5-methylcytosine than normal fibroblasts. Transfection of the gene encoding *Dnmt1* induced morphological transformation, whereas inhibition of *dnmt1* expression or activity resulted in reversion of *fos* transformation. Inhibition of histone deacetylase, which associates with methylated DNA, also caused reversion. These results suggest that *fos* may transform cells through alterations in DNA methylation and in histone deacetylation.

The *fos* proto-oncogene (*c-fos*) is the cellular homolog of the oncogene that is carried by the Finkel-Biskis-Jenkins (FBJ) murine sarcoma virus (1). Its protein product, Fos, is a nuclear phosphoprotein that forms heterodimeric complexes with Jun and activating transcription factor/cyclic adenosine 3',5'-monophosphate (cAMP) response element-binding protein family members and regulates transcription through activator protein-1 (AP1) and cAMP-responsive elements (1). Fos can be induced rapidly and transiently in many cells by diverse extracellular stimuli (2). It is believed to function in a transcription factor network that couples extracellular stimuli to alterations in gene expression. Gene disruption studies have shown that Fos is required for differentiation of oste-

oclasts, for oncogenic conversion of phorbol ester-induced skin tumors, and for light-induced death of photoreceptor cells in the eye (3). It is likely that the many heterodimeric

**Table 1.** Effect of *fos* transformation on the 5-methylcytosine content of DNA. The level of methylation relative to that in normal 208F cells (100%) was determined by high-performance liquid chromatography (HPLC) analyses of genomic DNA digested to nucleosides (26). DNA (10 µg per sample) was digested with deoxyribonuclease I, phosphodiesterase, and alkaline phosphatase, and the products were separated by HPLC. The data represent the average of three independent experiments (±SD), except for data from the 0.5% serum samples, which are from two experiments. Dash, not applicable.

Cellular source of DNA	Time of culture (hours)	Methylation (%)
CMV- <i>fos</i>	—	119 ± 4.9
FBJ/R	—	129 ± 4.7
LacI- <i>fos</i> + IPTG	24	110 ± 4.1
LacI- <i>fos</i> + IPTG	48	100 ± 5.9
LacI- <i>fos</i> + IPTG	72	97 ± 3.6
LacI- <i>fos</i> – IPTG	24	126 ± 4.1
LacI- <i>fos</i> – IPTG	48	132 ± 8.6
LacI- <i>fos</i> – IPTG	72	120 ± 2.4
LacI- <i>fos</i> – IPTG in 0.5% serum	72	116 ± 4.3
LacI- <i>fos</i> + IPTG in 0.5% serum	72	100 ± 3.8
CMV- <i>dnmt1</i>	—	167 ± 7.6

Department of Developmental Neurobiology, St. Jude Children's Research Hospital, Memphis, TN 38105, USA.

\*To whom correspondence should be addressed. E-mail: fos1@aol.com

complexes containing Fos regulate distinct target genes in different physiological contexts. Continuous expression of *fos* results in the morphological transformation of cultured rodent fibroblasts in vitro and the induction of bone tumors in mice (1, 4). Cell transformation requires the leucine-zipper and the DNA binding regions of *fos* (5). In transformed rat fibroblasts, the major partner of Fos is c-Jun, which was first described as the Fos-binding protein, p39 (6). Using a conditional expression system based on LacI, we demonstrated that a continuous period (~72 hours) of c-*fos* expression is required for complete morphological conversion, which occurs even in quiescent cells (7). Like other oncogenic transcription factors, *fos* is thought to transform cells by inappropriate regulation of gene expression (7, 8).

To identify target genes of *fos* that are effectors of cell transformation, we used representational difference analysis (RDA) (9) to isolate mRNA species, which are present in *fos*-transformed cells at levels that are higher than those present in normal fibroblasts. cDNA was prepared from LacI-*fos* cells, which contain a *fos* gene regulated by the LacI activator protein [comprising LacI, a nuclear localization signal, and the VP16 activator (7)], in the presence (normal phenotype) and absence (transformed phenotype) of isopropyl-β-D-thiogalactopyranoside (IPTG). In these cells, *fos* is rapidly repressed in the presence of IPTG and is rapidly induced in its absence. Although several *fos* target genes are induced within minutes of *fos* expression in these cells, transformation requires 2 to 3 days. The cDNA populations obtained from transformed and normal cells were used in RDA as tester and driver, respectively (10).

The difference products that were obtained after three rounds were analyzed by DNA sequencing and included the cathepsin L and aquaporin-1 genes (Fig. 1A) that were previously shown to be regulated by Fos or to contain AP1 regulatory elements (11, 12). In transformed cells, the candidate target genes were